Complexes of fullerenes C_{78} and $Sc_3N@C_{78}$ with concave receptors

E. M. Cabaleiro-Lago,[a] J. A. Carrazana-García[a], I. González-Veloso[b], J. Rodríguez-Otero[b]

[a] *Facultade de Ciencias (Dpto. de Química Física), Universidade de Santiago de Compostela, Campus de Lugo. Avda. Alfonso X El Sabio s/n 27002 Lugo, Galicia (Spain).*

[b] *CIQUS and Facultade de Química (Dpto. de Química Física), Universidade de Santiago de Compostela, 15782 Santiago de Compostela, Galicia (Spain).*

Abstract

A computational study is carried out regarding the characteristics of a set of fullerene complexes formed by the fullerene C_{78} and the endohedral fullerene $Sc_3N@C_{78}$ with a series of hosts of different nature, including corannulene, a zinc porphyrin and a chloro boron subphthalocyanine. The carbon cage is kept similar in these two fullerenes, so comparing the results obtained for their complexes will reveal the role of the endohedral cluster on modifying the characteristics of the fullerene and how it affects to the interaction.

Keywords:

Intermolecular interactions; concave-convex interaction; π-π interaction; fullerenes; endohedral fullerenes

1. Introduction

Non-covalent interactions involving fullerenes are usually dominated by dispersion, so potential hosts can be designed trying to maximize the contact area between host and guest, in most cases exploiting the so-called concave-convex π-π interactions.[1,2] One of the most obvious candidates for exploiting the concave-convex π-π interaction with fullerenes are buckybowls. These species are curved polycyclic aromatic hydrocarbons, the curvature arising from the impossibility of placing hexagons and pentagons in a planar sheet.[3] The simplest of these buckybowls, corannulene $C_{20}H_{10}$ has been the subject of study in recent years, also regarding its interaction with C_{60}. In fact, the well-known buckycatcher proposed by Sygula comprised two corannulene pincers held together by a cyclooctatriene tether.[4,5] This species is capable of catching fullerene just based on concave-convex π-π interactions. In our research group, the effect of extending the size of the bowl upon the interaction with fullerenes has been studied.[6-8] Annelating rings to corannulene results in more efficient receptors, especially when C-H···π contacts are possible. Also, enlarging the size of the bowl also favours the interaction with C_{60}, but some degree of flexibility has to be kept.

In the present work, the characteristics of the interaction of three host molecules (corannulene, a Zn porphyrin and a chloro boron subphthalocyanine (see Figure 1)) with the endohedral fullerene $Sc_3N@C_{78}$ and its pristine counterpart C_{78} are studied. $Sc_3N@C_{78}$ has been characterised as to having a carbon cage of D_3h symmetry.[9] Though of the 5 isomers of C_{78}, the D_3h one found in $Sc_3N@C_{78}$ is the least stable one,[10] this isomer will be considered in the present work in order to identify the effects due to the endohedral unit.

2. Computational Details

The most favourable structure of the dimers is selected by means of a pre-screening with the B97-D2[11,12] functional together with the def2-SVP basis set. After reaching a stationary point, complexation energies are computed at the B97-D2/def2-TZVP level of calculation, and the most stable structure found is selected for further reoptimization at the B97-D2/def2-TZVP level. Counterpoise-corrected complexation energies are obtained employing the def2-TZVP basis set and B3LYP[13,14] together with the D3 dispersion correction.[15-17] In all cases, the resolution of the identity approach has been employed in order to save computational time. In the case of the hybrid B3LYP method the chain of spheres approach has been employed for exchange (RIJCOSX).[18,19]

In order to gain more insight about the characteristics of the interaction in the dimers, the Non-Covalent Interaction Index (NCI) has been employed.[20,21] NCI is an index based on the analysis of the reduced density gradient that can be employed to visualize both favourable and unfavourable interactions. These interactions can be graphically displayed as a plot of the product of the sign of the second eigenvalue of the hessian of the density times the density ($\text{sign}(\lambda_2)\,\rho$), mapped onto an isosurface of reduced density gradient**.** All calculations have been performed with the Orca 3.03 program package.[22]

3. Results

Figure 1 shows the molecular electrostatic potentials of the host considered in this work. The curvature of corannulene produces an asymmetry on the charge distribution leading to a molecular dipole moment. As it can be observed in Figure 1, the MEP of corannulene is mostly negative by both faces, though it is more so by the convex side. The Zn porphyrin in Figure 1 also shows a negative electrostatic potential, with the exception of the region near the Zn atom. As expected, the subphthalocyanine shows a negative MEP by the convex face occupied by the chlorine atom, while the concave side of the molecule is mostly negative near the phenyl rings though with a central positive part near the boron atom.

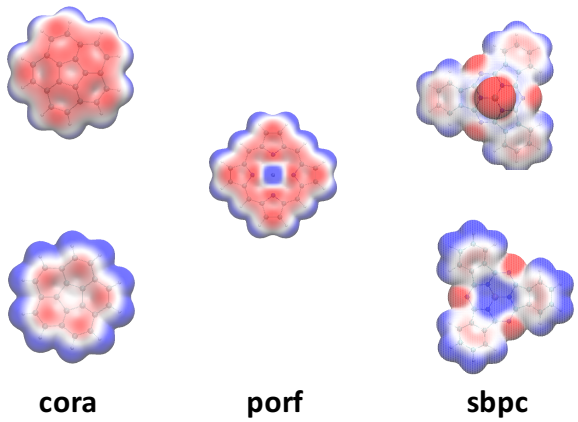

Figure 1. Molecular Electrostatic Potentials (MEP) at the B3LYP-D/def2-TZVP level (top and bottom views). MEP mapped onto an isodensity surface of 0.002 a.u. Colour scale runs from -0.020 a.u. (red) to 0.020 a.u (blue). White is 0.0.

Similarly, Figure 2 shows the MEPs obtained for the fullerenes C_{78} and $Sc_3N@C_{78}$, both sharing the same D_{3h} symmetry on the carbon cage. As usual with other fullerenes, the MEP of C_{78} is almost neutral or slightly positive. However, the presence of the endohedral cluster in $Sc_3N@C_{78}$ produces a more asymmetric arrangement of the charge leading to well-defined negative MEP regions located on the faces above and below the plane defined by the endohedral cluster, while the rest of the regions are similar to the pristine fullerene. On the right side of Figure 2 the differences between the MEPs of both fullerenes are shown, thus highlighting the impact of the endohedral cluster. It can be clearly observed how the regions above and below the plane of the cluster are more negative. Also, the regions where the scandium atoms interact with the carbon cage also display slightly more negative MEP than in the pristine fullerene. Therefore, the presence of the endohedral cluster promotes changes on the charge distribution leading to a fullerene cage which is overall more negative than that of the pristine fullerene, especially on the regions above and below the molecular cluster.

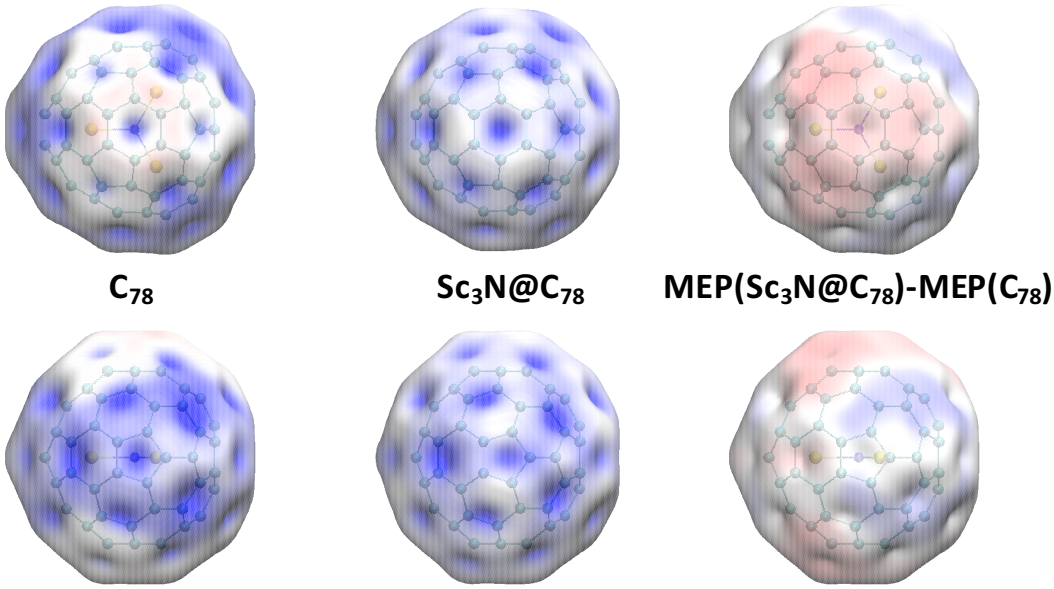

Figure 2. Molecular Electrostatic Potentials (MEP) at the B3LYP-D/def2-TZVP level. MEP mapped onto an isodensity surface of 0.002 a.u. Colour scale runs from -0.020 a.u. (red) to 0.020 a.u (blue). White is 0.0.

The Non-Covalent interaction Index (NCI) allows to display on a graphic way intermolecular interactions based on the characteristics of the charge density. However, it can also reveal the effects of the endohedral cluster in endofullerenes, as shown in Figure 3. In the case of C_{78} it can be observed that the unique features of the NCI 2D graph, are the red peaks corresponding to the ring critical points associated to the rings of the fullerene, together with the favourable blue region corresponding to the C-C bonds, appearing at densities around 0.18 a.u. However, the plot for $Sc_3N@C_{78}$ is markedly different, with a series of additional favourable peaks (in blue) corresponding to the interactions of the scandium atoms with the carbon cage, as well as to the N-Sc bonds (around density 0.08 a.u.). These differences are better observed in the plot at the bottom of Figure 3, where it can be observed that the features of C_{78} are also show in $Sc_3N@C_{78}$, corresponding to the carbon cage, but additional motifs appear revealing the interactions of the endohedral cluster with the cage, shown by the attractive interactions at around 0.05 a.u. These interactions can be also visualized in the 3D plot in Figure 4, where the clashes of the scandium atoms with the carbon cage are clearly displayed in red. However, the blue regions also indicate the presence of favourable interactions of scandium atoms with the cage.

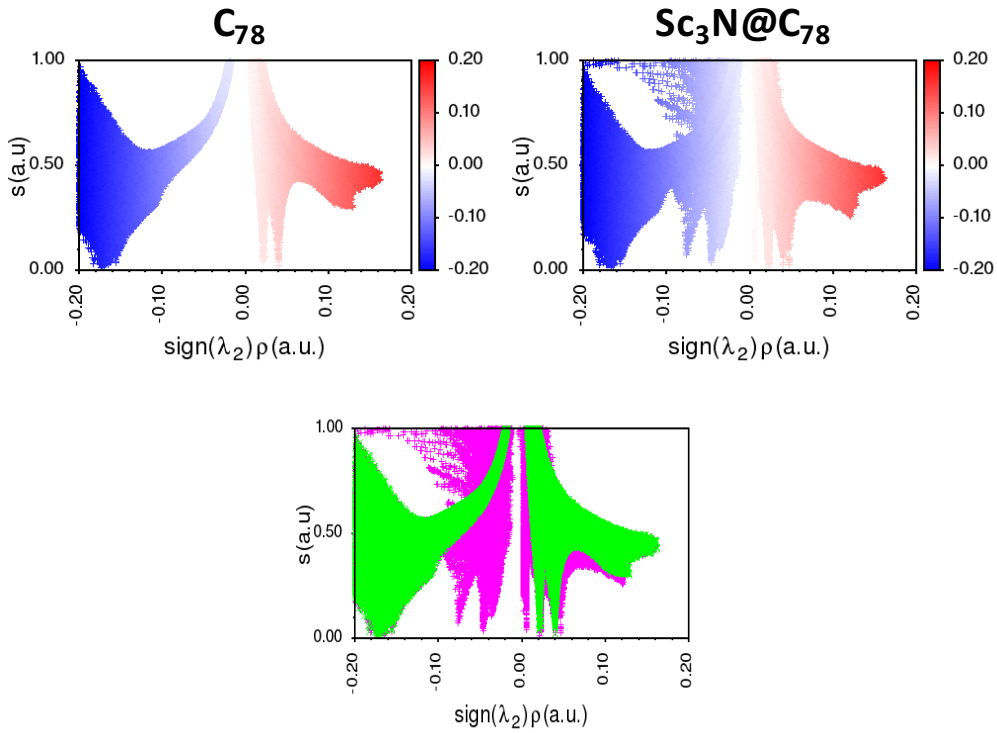

Figure 3. NCI plots for C_{78} and $Sc_3N@C_{78}$, the reduced density gradient is plotted against the product of the density times the sign of the second eigenvalue of its Hessian. At the bottom, the plot superimposes the NCI plots of C_{78} (green) and $Sc_3N@C_{78}$ (magenta).

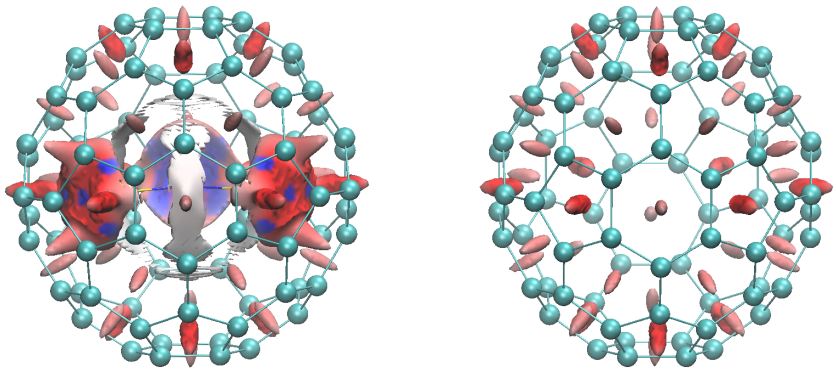

$Sc_3N@C_{78}$ **C_{78}**

Figure 4. NCI plots showing the interactions in fullerenes. The product of the density times the sign of the second eigenvalue of its Hessian is mapped onto an isosurface of reduced density gradient with value 0.4 a.u. The colour scale goes from −0.04 au (blue) to +0.04 au (red).

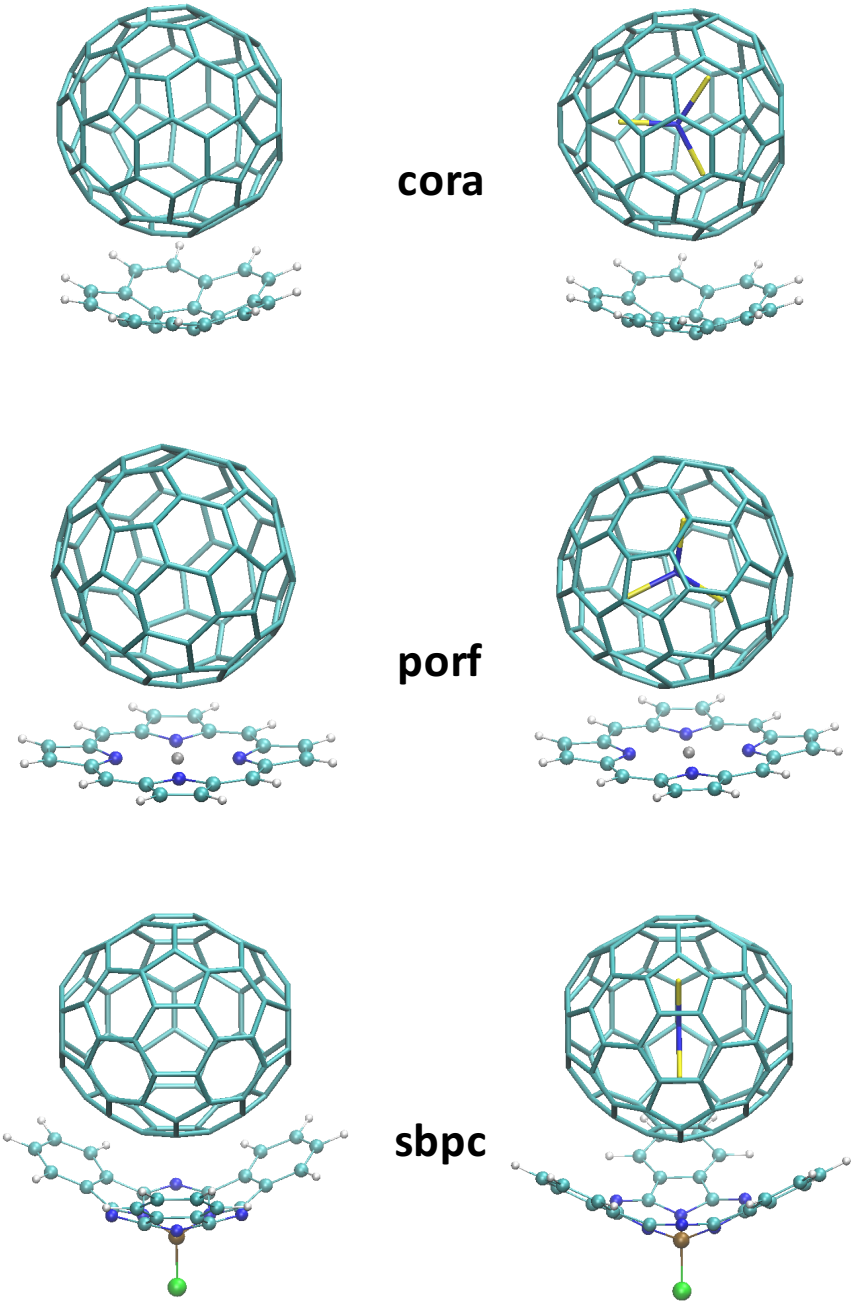

Figure 5. Most stable minima of the complexes formed with C_{78} (left) and $Sc_3N@C_{78}$ (right) as obtained at the B97-D2/def2-TZVP level.

Figure 5 shows the most stable structures found for the dimers studied. It can be observed that in the case of $Sc_3N@C_{78}$, the host molecules are located facing the region where the scandium atoms interact with the carbon cage. The distances between the geometrical centres of the molecules reflect the depth of the bowls, so they show shorter values in sbpc (5.9 Å) than in cora (6.4 Å) and porf (6.5 Å), see Table 1. Negligible differences are observed between complexes with pristine and endohedral fullerenes. However, the interaction is mostly controlled by dispersion, so the relevant parameter is the number of close contacts, which reflects the extent of the contacts between the surfaces of host and guest molecules. It can be observed in Table 1 that the average distance in contacts below 4.0 Å is similar in all cases, with a value around 3.6 Å. However, the number of contacts grows as we go from porf to cora and to sbpc, thus suggesting more favourable interactions in the latter. Also, it can be observed that the number of contacts decreases in complexes with $Sc_3N@C_{78}$, suggesting that the shape complementarity worsens as a consequence of the deformations of the cage induced by the endohedral unit.

Table 1. Geometrical parameters of the complexes studied. R_{centre} is the distance between geometrical centres of the molecules; R_{close} is the average distance for contacts below 4.0 Å, being N_{close} the number of these contacts.

	R_{centre} (Å)	R_{close} (Å)	N_{close}
cora-C_{78}	6.39	3.59	77
cora-$Sc_3N@C_{78}$	6.47	3.60	75
porf-C_{78}	6.53	3.63	72
porf-$Sc_3N@C_{78}$	6.52	3.60	73
sbpc-C_{78}	5.94	3.61	115
sbpc-$Sc_3N@C_{78}$	5.96	3.61	110

Table 2. Complexation energy (kcal/mol) for the most stable structures of the dimers studied at the B3LYP-D/def2-TZVP + 3-body dispersion correction**.**

	$\Delta E_{complexation}$	ΔE_{B3LYP}	$\Delta E_{dispersion}$	$\Delta E_{3\text{-}body}$
cora-C_{78}	-17.10	12.82	-31.32	1.40
cora-$Sc_3N@C_{78}$	-18.74	9.81	-30.08	1.53
porf-C_{78}	-18.26	11.39	-31.19	1.54
porf-$Sc_3N@C_{78}$	-18.54	12.57	-32.86	1.75
sbpc-C_{78}	-23.50	17.26	-42.89	2.13
sbpc-$Sc_3N@C_{78}$	-23.29	17.83	-43.52	2.40

Table 2 shows the complexation energies for the different complexes as obtained with the B3LYP-D method also including a three-body correction on the empirical dispersion model. As expected, the intensity of the interaction is larger in sbpc complexes as a consequence of the larger size of sbpc that leads to larger contact surfaces between sbpc and the fullerenes. On the other hand, despite the planarity of porf, its complexes are as stable as those obtained with cora, probably as a result of the interactions of the central Zn atom with the carbon cage. On the other hand, there seems that the presence of the endohedral cluster has no impact on the interaction energies, with values very close to those obtained with the pristine fullerene. This is compatible with an interaction dominated by dispersion; the endohedral atoms are too far away from the host molecule as to contribute significantly to dispersion. Despite these similar complexation energies, analysing the densities some differences appear. As shown in Figure 6, though the NCI plots for C_{78} and $Sc_3N@C_{78}$ are similar, new regions indicating weak favourable interactions appear, especially for sbpc and porf complexes. Therefore, the results indicate that the presence of the endohedral cluster has a limited impact on the stability of the complexes, though its effect onto other characteristics should be further tested.

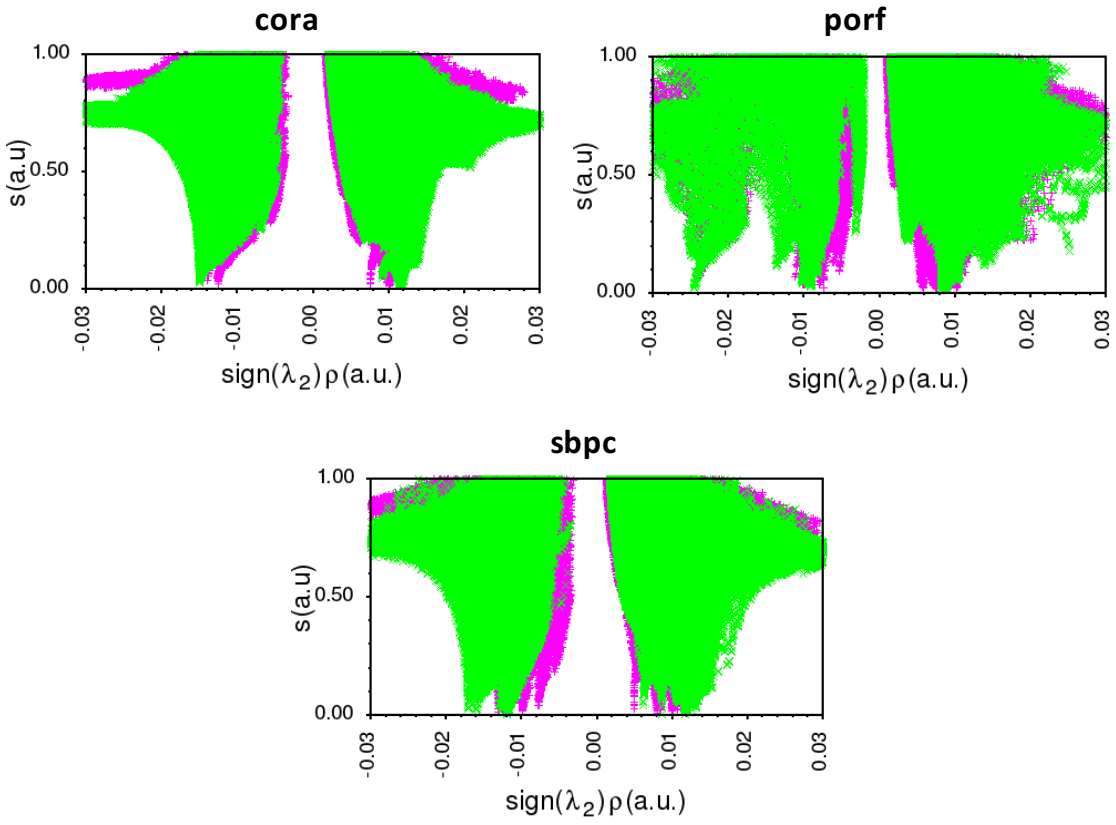

Figure 6. NCI plots comparing complexes with the different fullerenes. Green corresponds to C_{78} complexes and magenta to $Sc_3N@C_{78}$. The reduced density gradient is plotted against the product of the density times the sign of the second eigenvalue of its Hessian. Obtained with promolecular densities.

References

1. N. Martin; J.-F. Nierengarten. Supramolecular Chemistry of Fullerenes and Carbon Nanotubes; Wiley-VCH Verlag & Co. KGaA: Weinheim, Germany, **2012**.
2. E. M. Pérez; N. Martín. *Chem. Soc. Rev.* **2015**, *44*, 6425-6433.
3. M. A. Petrukhina; L. A. Scott. Fragments of fullerenes and carbon nanotubes; John Wiley & Sons, Inc.: Hoboken, New Jersey, **2012**.
4. L. Kobryn; W. P. Henry; F. R. Fronczek; R. Sygula; A. Sygula. *Tetrahedron Lett.* **2009**, *50*, 7124-7127.
5. C. Mueck-Lichtenfeld; S. Grimme; L. Kobryn; A. Sygula. *Phys. Chem. Chem. Phys.* **2010**, *12*, 7091-7097.
6. D. Josa; J. Rodríguez-Otero; E. M. Cabaleiro-Lago; L. A. Santos; T. C. Ramalho. *J. Phys. Chem. A* **2014**, *118*, 9521-9528.
7. D. Josa; L. Azevedo dos Santos; I. González-Veloso; J. Rodríguez-Otero; E. M. Cabaleiro-Lago; T. de Castro Ramalho. *RSC Advances* **2014**, *4*, 29826-29826.
8. D. Josa; J. Rodriguez-Otero; E. M. Cabaleiro-Lago. *Phys. Chem. Chem. Phys.* **2015**, *17*, 13206-13214.
9. A. A. Popov; L. Dunsch. *Chem. Eur. J.* **2009**, *15*, 9707-9729.
10. J. R. Colt; G. E. Scuseria. *Chem. Phys. Lett.* **1992**, *199*, 505-512.
11. S. Grimme. *J. Comput. Chem.* **2006**, *27*, 1787–1799.
12. S. Grimme. *J. Comput. Chem.* **2004**, *25*, 1463–1473.
13. C. Lee; W. Yang; R. G. Parr. *Phys. Rev. B* **1988**, *37*, 785-789.
14. A. D. Becke. *J. Chem. Phys.* **1993**, *98*, 5648-5652.
15. S. Grimme. *WIREs Comput. Mol. Sci.* **2011**, *1*, 211-228.
16. S. Grimme; J. Antony; S. Ehrlich; H. Krieg. *J. Chem. Phys.* **2010**, *132*, 214301.
17. S. Grimme; S. Ehrlich; L. Goerigk. *J. Comput. Chem.* **2011**, *32*, 1456-1465.
18. F. Neese; F. Wennmohs; A. Hansen; U. Becker. *Chem. Phys.* **2009**, *356*, 98-109.
19. R. Izsák; F. Neese. *J. Chem. Phys.* **2011**, *135*, 144105/144101.
20. J. Contreras-García; E. R. Johnson; S. Keinan; R. Chaudret; J.-P. Piquemal; D. N. Beratan; W. Yang. *J. Chem. Theory Comput.* **2011**, *7*, 625-632.
21. E. R. Johnson; S. Keinan; P. Mori-Sánchez; J. Contreras-García; A. J. Cohen; W. Yang. *J. Am. Chem. Soc.* **2010**, *132*, 6498-6506.
22. F. Neese. *WIREs Comput. Mol. Sci.* **2012**, *2*, 73-78.